Integrated modelling of thermal cycles, austenite formation, grain growth and decomposition in the heat affected zone of carbon steel

W. Zhang[1], J. W. Elmer[2] and T. DebRoy*[1]

The microstructure evolution in the heat affected zone (HAZ) of 1005 low carbon steel during gas tungsten arc welding (GTAW) was quantitatively investigated using a combination of several numerical models. In particular, the α ferrite$\rightarrow\gamma$ austenite phase transformation during heating was studied using a Johnson–Mehl–Avrami (JMA) analysis, the γ grain growth was calculated using a Monte Carlo simulation, and the $\gamma\rightarrow\alpha$ transformation during cooling was examined using an austenite decomposition model. In addition, the phase equilibria of the 1005 steel were calculated using computational thermodynamics software, Thermo-Calc, while the necessary temperature v. time data for all the microstructure models were obtained from a thermofluid model. These models were then used to calculate the extent of austenitisation with time during heating, the γ grain growth, and the volume fractions of various microconstituents of the final microstructure in the HAZ. It was found that a considerable amount of superheat was required for the initiation and completion of the $\alpha\rightarrow\gamma$ transformation under the heating rates typical of arc welding. Significant γ grain growth was found to take place in the HAZ, particularly in the vicinity of the fusion zone (FZ) boundary, where the computed maximum γ grain size was about eight times greater than that of the base metal. The predicted final microstructure in the HAZ was predominantly allotriomorphic and Widmanstatten ferrites, which was consistent with the post-weld metallographic measurements. Overall, the computed microstructure evolution in the HAZ using the multiphenomena models was consistent with the available experimental data. The results reported here indicate that it is now possible to develop a quantitative model of complex weld microstructure evolution with the recent advances in transport phenomena and phase transformation models.

Keywords: Austenite decomposition, Grain growth, JMA kinetics, Phase transformation, Welding

Introduction

It is well recognised that the final microstructure in the weldment results from a series of transformations during both weld heating and cooling.[1,2] For instance, during welding of low carbon steels, the typical microstructure history of the fusion zone (FZ) is α ferrite$\rightarrow\gamma$ austenite$\rightarrow\delta$ ferrite$\rightarrow$liquid$\rightarrow\delta$ ferrite$\rightarrow\gamma$ austenite$\rightarrow\alpha$ ferrite, while that of the heat affected zone (HAZ) is α ferrite$\rightarrow\gamma$ austenite$\rightarrow\alpha$ ferrite.[1] In the literature, the transformations during cooling, such as the $\gamma\rightarrow\alpha$ transformation, have been extensively investigated experimentally and theoretically. However, the transformations during heating have received relatively little attention. With the recent advances in experimental techniques, particularly using *in situ* synchrotron based X-ray diffraction techniques, phase transformations during weld heating can be directly observed.[3–7] Analyses of the X-ray diffraction data have provided much insight into the kinetics and mechanisms of transformations during heating.[3–11]

In the HAZ, a low carbon steel often undergoes three distinct events during the thermal cycle that determine its final microstructure. As shown in Fig. 1, the $\alpha\rightarrow\gamma$ transformation starts during heating above the A_1 temperature and continues until austenitisation is completed, which typically requires some superheat above the A_3 temperature. Rapid heating of the HAZ does not always allow equilibrium to be reached, owing to lack of time, and the extent of superheat is influenced

[1]Department of Material Science and Engineering, Pennsylvania State University, University Park, PA 16802, USA
[2]Chemistry and Materials Science Department, Lawrence Livermore National Laboratory, Livermore, CA 94551, USA

*Corresponding author, email debroy@psu.edu

Published by Maney on behalf of the Institute
Received 1 March 2005; accepted 11 April 2005
DOI 10.1179/174329305X48365

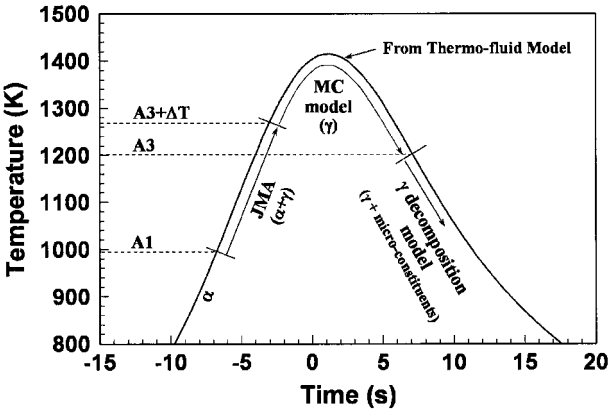

1 Main physical processes that are modelled to provide understanding of final microstructure in HAZ of 1005 steel during heating and cooling: austenitisation is modelled by Johnson–Mehl–Avrami (JMA) equation, grain growth of austenite is modelled by Monte Carlo (MC) model, and formation of final weld microstructure is modelled by austenite decomposition model; thermal cycle is modelled by heat and fluid flow model

by the heating rate. After the completion of austenitisation, the temperature continues to rise to the peak temperature before the cooling starts. Although the austenite grains start growing as soon as they form, the grain growth mainly occurs after the austenitisation is completed, since the rate of grain growth increases significantly with temperature. During cooling, austenite starts to decompose into various microconstituents below the A_3 temperature, and the process of decomposition depends strongly on the cooling rate and austenite grain size. The final microstructure of the HAZ results from multiple physical phenomena that occur during heating and cooling, i.e. the $\alpha \rightarrow \gamma$ transformation during heating, the γ grain growth, and the $\gamma \rightarrow$microconstituents transformation(s) during cooling. Furthermore, the kinetics of phase transformations during heating and cooling as well as the grain growth depend on the thermal cycle. Therefore, any quantitative understanding of the final microstructure must include these events. Most previous studies on the quantitative understanding of the evolution of microstructure in the HAZ were focused on the individual physical processes that result in the final microstructure. Synthesis of these component processes was usually not attempted because of the complexity of the task.

Here we show that various numerical models available in the literature can be combined to provide understanding of the complex microstructure evolution in the weldment because of the recent advances in the computational hardware and software. In particular, a thermofluid model, a thermodynamics model, models for the phase transformations during heating and cooling and a model for the austenite grain growth are combined to provide understanding of the evolution of microstructure in the HAZ during welding. AISI 1005 low carbon steel is chosen as the model system, since extensive experimental and theoretical studies have been carried out that have yielded reliable models of the component physical processes that take place during welding.[9–11] In particular, the $\alpha \rightarrow \gamma$ transformation during heating, the γ grain growth and the $\gamma \rightarrow \alpha$ transformation during cooling have been quantitatively investigated. Comparison of independent experimental results with the results obtained from the overall model, created by integrating the individual models, showed good agreement between the calculated results and the experimental measurements. The task of assimilating several component models, although fairly complex, was found to be both a realistic and a promising venture, since the integration of multiple numerical models provided fairly reliable results. The predictions of the superheat for the completion of austenitisation, the prior γ grain size and the volume fractions of various microconstituents in the final microstructure of the HAZ represent a contribution to the growing quantitative knowledge base of fusion welding.

Welding conditions

Circumferential autogenous welds were made on AISI 1005 cylindrical steel bars, 10·8 cm in diameter and 12·7 cm long, by gas tungsten arc (GTA) welding in an environmentally sealed chamber to avoid atmospheric contamination of the weld. The composition of as received bar was 0·05C–0·31Mn–0·18Si–0·11Ni–0·10Cr–0·009P–0·008Cu–0·005S–<0·005Al–<0·005Nb–<0·005Mo–<0·005Ti–<0·005V (wt-%). The welds were made using a constant power of 1·9 kW (110 A, 17·5 V) with a W–2Th welding electrode measuring 4·7 mm in diameter. High purity (99·999%) helium was used as both the welding and shielding gas. The steel bar was rotated below the fixed electrode at a constant speed of 0·11 rev min^{-1}, which corresponds to a surface welding speed of 0·6 mm s^{-1}.

Mathematical models

The following models are utilised in the present work: a weld thermofluid model[8–13] to calculate the thermal cycles, the Thermo-Calc software to calculate the phase equilibria,[3] a Johnson–Mehl–Avrami (JMA) kinetic formulation[8–11] to predict the kinetics of $\alpha \rightarrow \gamma$ transformation during heating, a Monte Carlo (MC) model[14–18] to calculate the γ grain growth, and an austenite decomposition model[19–21] to examine the kinetics of $\gamma \rightarrow \alpha$ transformation during cooling. Equilibrium phase diagrams provide the basis for understanding the phase transformations under welding conditions. The computational thermodynamics software, Thermo-Calc, was used to calculate the phase equilibria in the 1005 steel.[3] The resulting equilibrium phase transformation temperatures were then used in the three weld microstructure models. The JMA analysis, the MC simulation and the austenite decomposition model were coupled in a sequential manner, as discussed in the following section.

Calculation of weld thermal cycles

Weld thermal cycles were calculated using a well tested three-dimensional numerical heat transfer and fluid flow model described in detail in the literature for a flat plate geometry.[12,13] No significant error was introduced due to the heat transfer calculations in the flat geometry, since the weld pool dimensions were much smaller than the dimensions of the cylindrical bar. The equations of conservation of mass, momentum and energy in three-dimensional form were discretised and solved numerically by a form of Gaussian elimination method.[8,13] The

weld pool boundary, i.e. liquid/solid interface, is traced using an enthalpy–porosity technique in a fixed Cartesian coordinate system. The calculations take into account the electromagnetic, surface tension gradient and buoyancy driving forces present in the transient weld pool convection. In addition, at the weld top surface, the heat loss due to the helium shielding gas is considered by using Newton's law of cooling with an appropriate heat transfer coefficient. In this model, the transient problem is transformed into a steady-state problem by using a coordinate system moving with the heat source.[8,13] A $77 \times 40 \times 49$ grid system was used in the calculation, and the corresponding computational domain was 163 mm in length, 60 mm in width and 42 mm in depth. After the steady-state temperature field was obtained, the thermal cycle at any given location was calculated from the temperature field and the welding velocity. The weld thermofluid model and the computed thermal cycles in the 1005 arc welds have been reported in several previous publications.[8,13] Therefore, the details of the thermofluid model are not repeated here. The material property data and welding parameters used in the calculations are presented in Table 1.

Post-weld metallographic examination indicated that the weld FZ was elliptical in shape, with a half-width of 4·5 mm and a depth of 1·8 mm.[8,10] Macrographs of the FZ have been given in the literature[8–10] and are not presented here. This wide and shallow FZ is typical in steel arc welds, where the heat transfer within the weld pool occurs mainly by convection and the Peclet number is much larger than 1. Consideration of heat conduction alone cannot explain the observed weld pool geometry. The computed weld pool half-width of 4·4 mm and depth of 1·8 mm agreed very well with those determined metallographically, indicating the accuracy of the thermofluid model for the calculation of the temperature fields and thermal cycles.

Ferrite to austenite transformation during heating

In order to model the kinetics of the $\alpha \rightarrow \gamma$ transformation, the JMA approach is used to quantitatively describe the overall transformation rate. This approach can be represented by the following expression[22]

$$f_e(t) = 1 - \exp[-(kt)^n] \quad (1)$$

where $f_e(t)$ is the extent of the transformation at a given time t, n is the JMA exponent, and k is a rate constant given as

$$k = k_0 \exp\left(-\frac{Q}{RT}\right) \quad (2)$$

where k_0 is a pre-exponential constant, Q is the activation energy of the transformation, including the driving forces for both nucleation and growth, R is the gas constant, and T is the absolute temperature in K. For simplicity, it is assumed that the kinetic parameters Q, k_0 and n are independent of temperature; that is, there is no significant change in the nucleation and growth mechanisms during the phase transformation.[22] These assumptions are reasonable for the 1005 steel, since the base metal microstructure largely consists of equiaxed ferrite grains. It is expected that all the available nucleation sites will be consumed at the beginning of the $\alpha \rightarrow \gamma$ transformation and the transformation is then controlled by the carbon diffusion.

Equation (1) is further modified to derive the JMA-based expression applicable to non-isothermal phase transformations occurring in the $\alpha + \gamma$ two phase region. This modelling approach was combined with the calculated thermal profiles and the spatially resolved X-ray diffraction (SRXRD) experimental data to determine the JMA parameters. The resulting kinetic parameters are useful in determining the transformation rates under various heating conditions. More details of the JMA approach are available in the literature.[8–11]

In the present work, the γ grain growth is assumed to take place only in the portion of the HAZ where the $\alpha \rightarrow \gamma$ transformation has gone to completion and has created a single phase austenitic region. This assumption is reasonable, in that the untransformed α phase in the $\alpha + \gamma$ region may hinder the growth of the γ grains. In other words, the γ grain growth is retarded by the untransformed α, since the γ boundary migration is 'pinned' by the presence of the α grains. Using equation (1) and the computed thermal cycles, the regions of the HAZ where α transforms completely into γ during heating can be quantitatively determined. The kinetics of γ grain growth in the single γ region are then determined using the MC simulation, as discussed in the following section.

Table 1 Material property data and welding conditions used in the weld thermofluid model for the calculation of velocity and temperature fields[8]

Data	Value
Liquidus temperature, K	1802
Solidus temperature, K	1779
Density of liquid metal, kg m^{-3}	$7{\cdot}2 \times 10^3$
Effective viscosity of liquid, kg m^{-1} s^{-1}	0·1
Thermal conductivity of solid, J m^{-1} s^{-1} K^{-1}	36·4
Effective thermal conductivity of liquid, J m^{-1} s^{-1} K^{-1}	102·2
Specific heat of solid, J kg^{-1} K^{-1}	754
Specific heat of liquid, J kg^{-1} K^{-1}	754
Latent heat of melting, J kg^{-1}	$2{\cdot}7 \times 10^5$
Temperature coefficient of surface tension, N m^{-1} K^{-1}	$-0{\cdot}49 \times 10^{-3}$
Arc current, A	110
Arc voltage, V	17·5
Welding speed, m s^{-1}	6×10^{-4}

Austenite grain growth

After completion of the $\alpha \rightarrow \gamma$ transformation during heating, the transformed γ grain may start to grow. An existing three-dimensional MC model[14–18] was used to simulate the kinetics of γ grain growth. The model takes into account the non-isothermal heating conditions, the high spatial temperature gradient present in the weldment (the so-called 'thermal pinning' effect) and the effect of grain topological features. The MC model is discussed in detail elsewhere,[14–18] and Table 2 summarises the input data used in the calculations.[23]

There are two prerequisites for using the MC model: the physical boundaries of the single γ region and the initial γ grain size immediately after the $\alpha \rightarrow \gamma$ transformation. The former can be determined using the JMA equation and thermal profiles, as discussed previously.

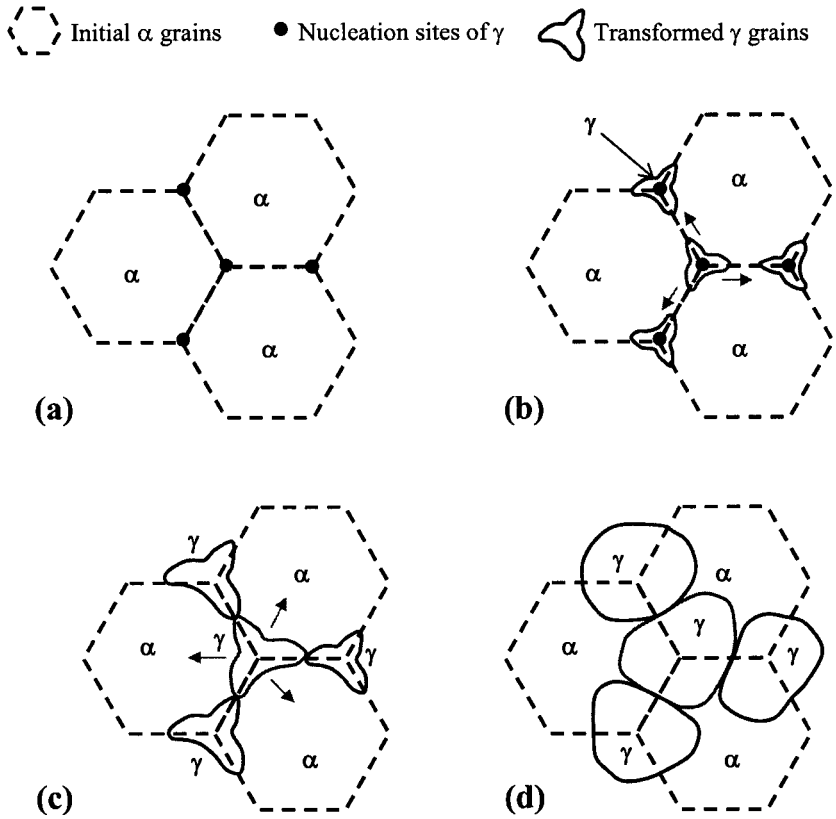

a Starting α grain structure; *b* Initial nucleation and growth of γ grains; *c* Growth of γ grains; *d* γ grain structure just before the completion of the transformation

2 The assumed sequence of $\alpha \rightarrow \gamma$ transformation during heating; the solid arrows indicate the primary directions of γ growth

The latter can be estimated from the starting grain size of base metal microstructure. The base metal of the 1005 steel largely consists of equiaxed α grains with a known grain size.[3,8] For simplicity, the equiaxed α grains in the base metal can be approximated by hexagons in two dimensions,[2] as shown in Fig. 2*a*. Previous JMA analyses suggested that the $\alpha \rightarrow \gamma$ transformation during heating is controlled by growth with zero nucleation rate,[8–10] whereby the γ nucleation sites are consumed at the beginning of this transformation. Therefore, it is reasonable to assume that the γ phase nucleates simultaneously at all the ferrite grain boundary triple points (indicated by the solid dots), because the location of the pearlite in the starting microstructure and these sites are the most energetically favourable sites for nucleation to occur.[22] Once nucleated, the γ grains start growing into the α phase, as shown in Fig. 2*b*. The γ grain will grow preferentially along the α grain boundaries, which offer a rapid diffusion path for carbon atoms, until the neighbouring γ grains impinge on each other, as shown in Fig. 2*c*. Subsequently, the γ grains grow inside the parent α grains. Hence, for this type of transformation, it may be reasonable to assume that the initial mean size of the γ grains is approximately half that of the parent α grains, since on average each of the six nucleation sites per α grain is shared by three resulting γ grains, as shown in Fig. 2*d*.

Table 2 Data used in MC calculation of γ grain growth in 1005 steel[23]

Property	Value
Thermal conductivity of solid k_S, W m^{-1} K^{-1}	36·4
Specific heat per unit volume ρC_P, J m^{-3}	$5{\cdot}8 \times 10^6$
Solidus temperature T_S, K	1779
Activation energy of grain growth, J mol^{-1}	$1{\cdot}8 \times 10^5$
Experimental grain growth exponent n	3·17
Pre-exponential factor for grain growth	$2{\cdot}19 \times 10^{-3}$
Grain boundary energy, J m^{-2}	1·77
Initial γ grain size, μm	10·8

Austenite decomposition during cooling

Based on thermodynamics and phase transformation kinetics, Bhadeshia *et al.*[19,20] developed an austenite decomposition model, which can predict the time–temperature transformation and continuous cooling transformation diagrams for the $\gamma \rightarrow \alpha$ transformation during cooling of low alloy steel welds. Together with the computed cooling rates, their model can calculate the volume fractions of various weld metal microstructures such as the allotriomorphic and Widmanstatten ferrites. Details of this model are available in the literature.[19–21] Although the austenite decomposition model was developed to predict the microstructure in the FZ, this model is extended for the calculation of the final microstructure in the HAZ because the austenite decomposition in the single γ region of the HAZ is quite similar to that in the FZ. Furthermore, because no liquid forms in the HAZ, the γ grain size can be more accurately calculated in the HAZ. Allotriomorphic ferrite is the first phase to form from the γ phase during cooling. It nucleates along the γ grain boundaries and grows by diffusion.[19–21] As the temperature decreases,

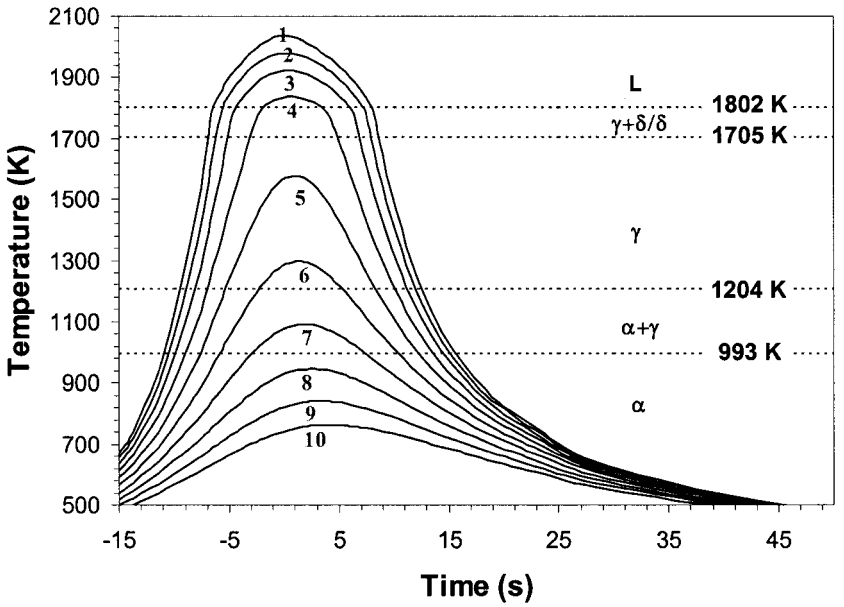

3 Computed thermal cycles at various distances from the weld centre. 1, 0 mm; 2, 2 mm; 3, 3 mm; 4, 4 mm; 5, 5 mm; 6, 6 mm; 7, 7 mm; 8, 8 mm; 9, 9 mm; 10, 10 mm. δ and L represent the δ ferrite and liquid, respectively. Superimposed are the equilibrium temperatures of various transformations in the 1005 steel computed using Thermo-Calc. Welding parameters are summarised in Table 1

the growth rate of allotriomorphic ferrite decreases, and the growth of allotriomorphic ferrite finally gives way to the growth of Widmanstatten ferrite. Widmanstatten ferrite nucleates either directly from the austenite grain surfaces or indirectly from allotriomorphic ferrite/austenite interfaces. At even lower temperatures, the remaining austenite transforms into bainite or martensite, depending on the cooling rate.[19–21] In the $\alpha+\gamma$ two phase region, the austenite decomposition will take place by a different mechanism from that in the single γ region of the HAZ, since the untransformed α phase can grow directly into the γ phase so that no nucleation of the α phase is needed.[2]

In addition to the steel chemical composition and the cooling rates, the austenite decomposition model requires knowledge of the average size of the prior γ grain. In the HAZ, the prior γ grain size was determined using the MC simulation described in the previous section. The prior γ grains in the FZ are assumed to have a uniform size,[19–21] and the average grain size was determined metallographically from the weld cross-sections.[8]

In short, the three microstructure models were coupled in the following manner. As shown in Fig. 1, at first, the JMA equation was used to calculate the kinetics of the $\alpha\rightarrow\gamma$ transformation during heating, and the location of the single γ phase region was determined. Next, the γ grain growth in the single γ phase region was calculated using the MC model, and the γ grain size prior to the $\gamma\rightarrow\alpha$ transformation was determined. The prior γ grain size and cooling profiles were then used in the austenite decomposition model to predict the final microstructure in the weldment.

Results and discussion

Computed weld thermal cycles

The temperature *v.* time data at various locations in the weldment are necessary for understanding of the microstructure evolution during welding. The computed thermal cycles in different locations at the weld top surface of the 1005 steel are shown in Fig. 3. As shown in this figure, the peak temperatures and heating and cooling rates at various locations decrease with increasing distance from the welding centreline. The equilibrium temperatures of phase transformations calculated using Thermo-Calc® are superimposed in Fig. 3. These equilibrium temperatures, together with the computed thermal cycles, provide useful information about the phase transformations under welding conditions. For example, Fig. 3 indicates that the peak temperature at location $y=2$ mm (i.e. curve 2) is well above the liquidus temperature. Hence, it undergoes melting during heating and solidification during cooling. On the other hand, at location $y=5$ mm (i.e. curve 5), the peak temperature is below the liquidus temperature, and it only experiences various solid-state transformations. Since the temperature at this location is above the A_3 temperature (1204 K), it is expected that this location experiences the complete $\alpha\rightarrow\gamma$ transformation during heating, γ grain growth, and finally $\gamma\rightarrow\alpha$ transformation during cooling. Further away from the weld centreline, say at $y=8$ mm (i.e. curve 8), the peak temperature is lower than the A_1 temperature (993 K). Hence, at this location, there will be no transformation to γ; however, annealing phenomena may occur. It should be noted that the above analysis, based on equilibrium temperatures only, provides qualitative information about the possible phase transformations taking place during welding.

In a typical weld, the temperature contours are compressed ahead of the weld pool and expanded behind it. The heating rate is determined by the extent of compression of the temperature contours and the welding speed. In Fig. 3, the weld travel speed (0·6 mm s^{-1}) was much lower than that in most typical GTA welding processes. As a result, the computed heating rates were lower than those for a typical welding conducted at a higher welding speed. Furthermore, the low welding speed also resulted in the somewhat symmetrical temperature–time plot in Fig. 3.

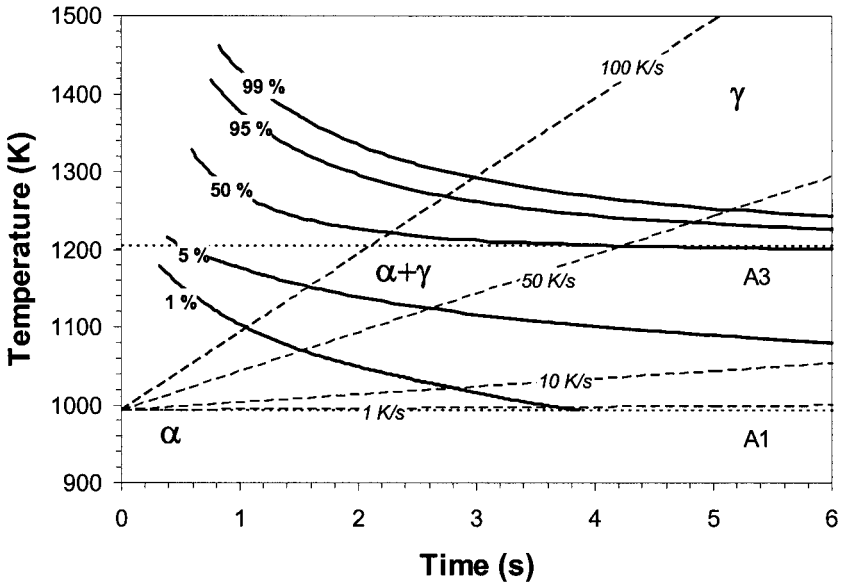

4 Calculated CHT diagram for the $\alpha \rightarrow \gamma$ transformation during heating of 1005 steel. Kinetic parameters used in the calculation were determined from the X-ray diffraction data[10]

Understanding the extent of different transformations depends on the transformation kinetics, which are simulated using various microstructure models as discussed in the following sections.

Kinetics of $\alpha \rightarrow \gamma$ transformation during heating

Figure 4 shows the computed continuous heating transformation (CHT) diagram obtained using the JMA equation and the kinetic parameters of Q= 117·1 kJ mol^{-1}, n=1·45 and ln k_0=12·2 previously determined based on the SRXRD data acquired for GTA welds in 1005 steel.[10] Superimposed are the A_1 (993 K) and A_3 (1204 K) temperatures for the 1005 steel as calculated by Thermo-Calc®.[3] As shown Fig. 4, the transformation rate increases rapidly with temperature, and the start and finish temperatures of the transformation both increase with increasing heating rate. The CHT diagram for the 1005 steel indicates that for the isothermal formation of austenite, the transformation start time is usually greater than 1 s, while the time for completion is greater than 10 s. In addition, it is apparent that some amount of superheat is required to start and complete the phase transformation under non-isothermal conditions. For example, for a heating rate of 80 K s^{-1}, Fig. 4 indicates that a superheat of about 66 K above the A_3 temperature is predicted for the completion of the transformation.

Kinetics of γ grain growth

As discussed previously, appreciable γ grain growth takes place mainly after completion of the $\alpha \rightarrow \gamma$ transformation. In this study, a temperature of 1270 K was used to represent the starting temperature of the γ grain growth in the entire HAZ, since the typical heating rates in the HAZ are around 80 K s^{-1}, requiring a superheat of 66 K above the A_3 temperature to complete the transformation to γ. It should be noted that the actual completion temperature of the $\alpha \rightarrow \gamma$ transformation depends on the local heating rate, and varies between different locations in the HAZ. However, using a constant temperature for representing the start of γ grain growth is reasonable, since the grain growth is a thermally activated process and the majority of growth takes place at elevated temperatures.[14–18]

Figure 5 shows the γ grain structure at the weld top surface calculated using MC simulation. This snapshot was taken just prior to the γ decomposition during cooling. As shown in Fig. 5, a spatial gradient of γ grains exists in the HAZ: the closer to the FZ, the larger the grain size, and vice versa. Such spatial grain size variation results from the local variation of thermal cycles and peak temperatures. As shown in Fig. 5, two microstructure subregions can be identified in the HAZ: the coarse grain region (CGR) and the fine grain region (FGR). The CGR, located near the FZ boundary, is subjected to strong thermal cycles in the HAZ. As a result, significant γ grain growth takes place in the CGR and large γ grains form. At a location about 1·2 mm away from the FZ boundary, the peak temperature is just slightly higher than the A_3 temperature (see curve 6 in Fig. 3). Therefore, the transformed γ grains are 'frozen', and very little grain growth occurs in the FGR.

Figure 6 shows the calculated mean γ grain size as a function of distance from the FZ boundary at the weld top surface and the vertical symmetry plane for the 1005 steel weld. The broken line represents the average grain size of the base metal, which consists of mainly equiaxed α grains. As shown in Fig. 6, the computed maximum γ grain size at the location adjacent to the fusion boundary is almost eight times higher than the initial size. The grain size decreases with distance from the fusion boundary, reaching a point (A_{yy}' and A_{zz}') where the grains become smaller than the base metal grains. At the location further away from the FZ boundary (B_{yy}' and B_{zz}'), the $\alpha \rightarrow \gamma$ transformation during heating does not initiate, since the peak temperature at this location is lower than the A_1 temperature (see curve 8 in Fig. 3). Therefore, no γ exists beyond location B. The area between locations A and B defines a region where the γ grain size is less than that of the base metal, i.e. a fine grain region. The FGR experiences a relatively low temperature history. As a result, in the FGR, either a partial transformation to γ has taken place or the

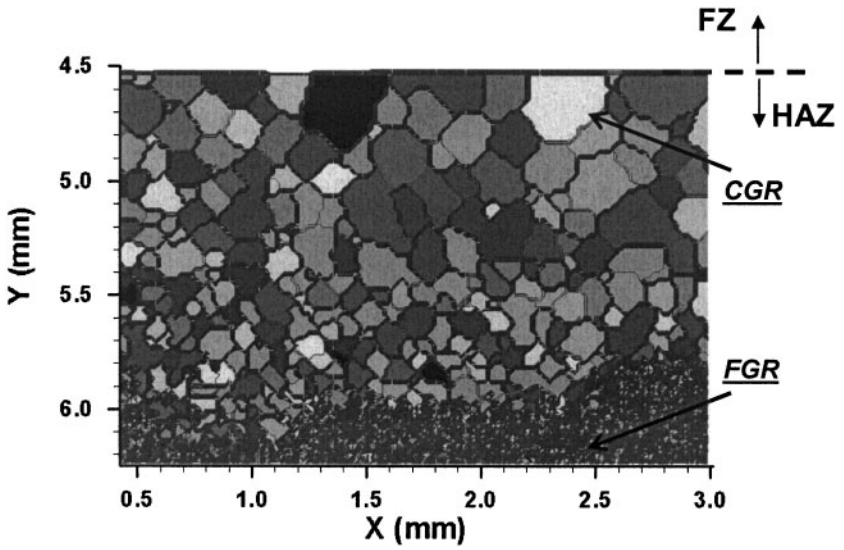

5 Computed γ grain structure at the weld top surface prior to the austenite decomposition during cooling. CGR and FGR represent, respectively, the coarse grain region and fine grain region after the γ grain growth

transformed γ is unable to grow due to low temperature. The FGR modelled using the MC simulation is consistent with the post-weld metallographic observations in the 1005 arc weld.[3,8] Additional transformations that occur during weld cooling can further refine these grains, and require additional modelling.

The MC calculations can be compared with diagrams based on experimental data for grain growth in steels, as indicated by the diamond symbols in Fig. 6. These data are obtained from a HAZ grain growth diagram for C–Mn steels.[2,24] The grain growth diagram was calibrated so that the diagram predictions matched the experimental measurements.[2] For a given heat input, the grain growth diagram provides the γ grain size as a function of peak temperature. The diamond symbols in Fig. 6 show the γ grain size distribution along the ZZ' direction obtained from the grain growth diagram. As shown in Fig. 6, the grain sizes computed using the MC simulation are in good agreement with those from the grain growth diagram, which is based on experimental data, indicating the validity of the MC simulation. The accuracy of the MC technique originates from its ability to calculate grain growth in a topologically connected network[14–18] and its consideration of the thermal pinning effect[15,16] resulting from the existence of strong spatial gradients of temperature.

Kinetics of austenite decomposition during cooling

Using the calculated γ grain sizes shown in Fig. 6 and the computed cooling rates, the final microstructure at various locations in the HAZ was determined, and the results are plotted in Fig. 7. These results show the

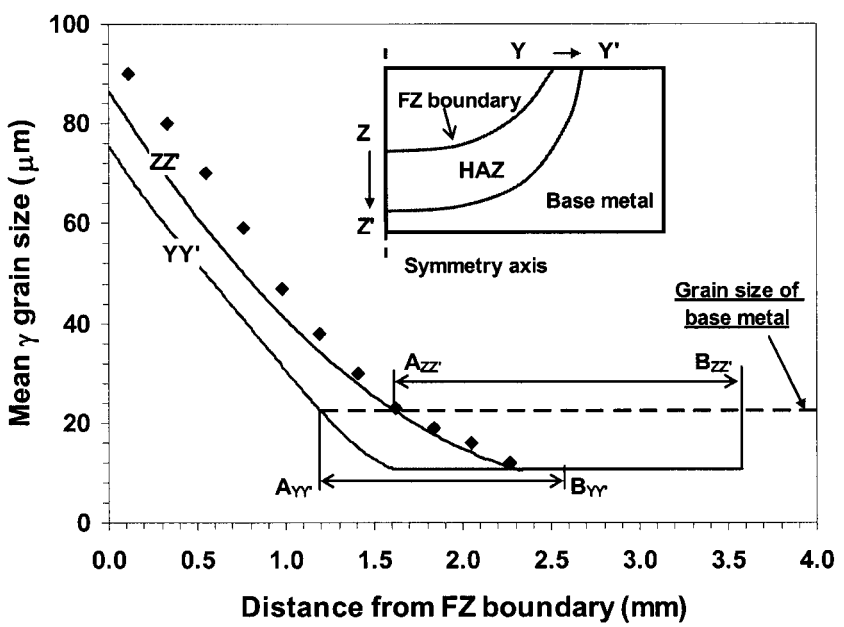

6 Calculated mean γ grain size as a function of distance from the FZ boundary using the MC model. YY' and ZZ' represent the directions along the weld top surface and the vertical symmetry plane, respectively, as shown in the inset figure. The diamond symbols represent the grain size distribution for steel welds obtained from the available grain growth diagram

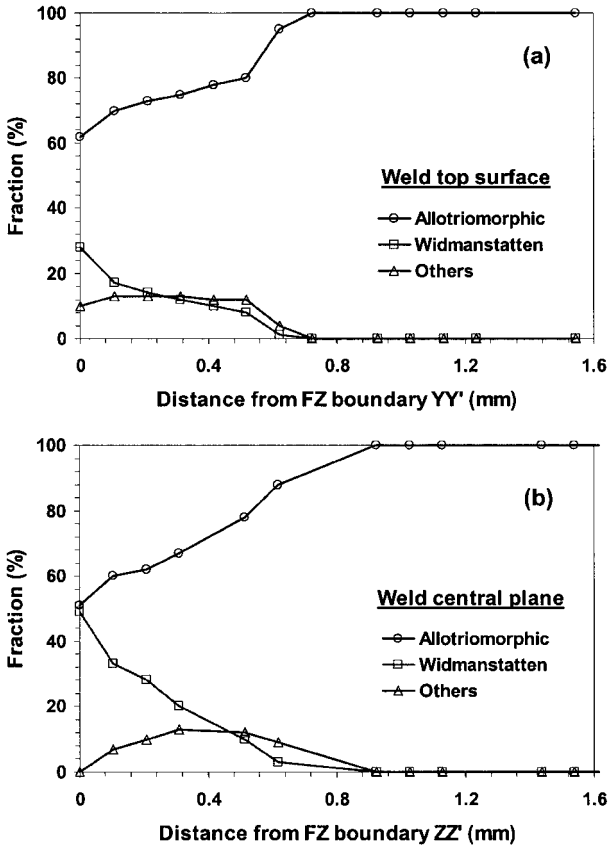

a Weld top plane; *b* symmetry plane

7 Spatial variation of the final microstructure in the HAZ location where the α completely transforms into γ during heating. The YY' and ZZ' directions are shown in the inset plot of Fig. 6. Far away from the FZ boundary and in the base metal, the microstructure consists of equiaxed ferrite grains with a small amount of pearlite, which are not shown in this figure

spatial variation of the various microstructural constituents in the HAZ. These microconstituents are primarily allotriomorphic and Widmanstatten ferrites, which is consistent with the experimental observations.[8] As the distance from the FZ boundary increases, the fraction of the allotriomorphic ferrite increases, whereas that of Widmanstatten ferrite decreases. This is due to the spatial variation of the prior γ grain size in the HAZ, which decreases away from the FZ boundary. The fraction of allotriomorphic ferrite depends inversely on the prior γ size for a given thickening rate. Since the spatial variations of composition and cooling rates are small, the thickening rate of the allotriomorphic ferrite layer in the HAZ is expected to be roughly constant. As a result, the larger the prior γ grain size, the smaller the fraction of allotriomorphic ferrite. Widmanstatten ferrite grows after the completion of the γ to allotriomorphic ferrite transition, and its fraction is thus limited by the remaining γ phase. It is interesting to note that at a distance about 0·8 mm from the FZ boundary, the prior γ size is small enough for the γ phase to completely transform into allotriomorphic ferrite.

Grong investigated the effect of the prior austenite grain size on the allotriomorphic ferrite in an Nb microalloyed steel.[2] It was found that the amount of allotriomorphic ferrite depended strongly on the austenite grain size. A coarse austenite of 150 μm results in 1% of allotriomorphic ferrite, while a fine austenite of 10 μm results in 90% of allotriomorphic ferrite.[2] It seems that the HAZ microstructure distribution predicted using the austenite decomposition model is consistent with Grong's findings.[2]

Summary and conclusions

Microstructure evolution during GTA welding of the 1005 low carbon steel was studied using a multi-phenomena modelling framework synthesising a weld thermofluid model, computational thermodynamics software, a JMA analysis, an MC simulation and an austenite decomposition model.

1. The JMA analysis considers the non-isothermal heating and transformation in the $\alpha+\gamma$ two phase field. Using the JMA kinetic parameters previously determined for 1005 steel arc welds (Q=117·1 kJ mol^{-1}, n=1·45 and ln k_0=12·2), the kinetics of the $\alpha\rightarrow\gamma$ transformation are calculated for various heating conditions. It is found that a considerable amount of superheat is required for the initiation and completion of the phase transformation under the heating rates common to arc welding.

2. The MC model is used to calculate the kinetics of the γ grain growth in the HAZ. It is found that significant γ grain growth takes place in the HAZ, particularly in the vicinity of the FZ boundary. The computed maximum γ grain size is found to be about eight times greater than that of the base metal. The calculated prior γ grain size distribution is in fair agreement with that available in the literature. The γ grain size is used for understanding the final microstructure in the weldment.

3. The transformation of austenite to various ferrite microconstituents during cooling is examined using the austenite decomposition model. The predicted final microstructure in the weldment is predominantly allotriomorphic and Widmanstatten ferrites, which is consistent with the post-weld metallographic measurement. The spatial variation of the final microstructure in the HAZ is quantitatively determined. It is found that the volume fraction of allotriomorphic ferrite increases, while that of the Widmanstatten ferrite decreases, as the distance to the FZ boundary increases.

The results presented here illustrate that the microstructure evolution during welding can be examined by the combination of various microstructure models and the computed thermal cycles. Further experiments are needed to extend this integrated weld modelling approach to more complex alloy systems, where the kinetics of the phase transformations differ from those of the 1005 steel studied here.

Acknowledgements

The Pennsylvania State University portion of the work was supported by a grant from the US Department of Energy, Office of Basic Energy Sciences, Division of Materials Sciences, under grant number DE-FGO2-01ER45900. The LLNL portion of this research was performed under the auspices of the US Department of Energy, Lawrence Livermore National Laboratory, under Contract No. W-7405-ENG-48. Dr Zhang gratefully acknowledges the award of a Fellowship from the American Welding Society. The authors would like to

thank Mr S. Mishra for his help in and useful discussion of the grain growth calculations. The authors are grateful to Professor H. K. D. H. Bhadeshia for help with the microstructure calculations.

References

1. K. Easterling: 'Introduction to the physical metallurgy of welding', 2nd edn; 1992, Oxford, Butterworth-Heinemann.
2. Ø. Grong: 'Metallurgical modeling of welding', 2nd edn; 1997, London, The Institute of Materials.
3. J. W. Elmer, J. Wong and T. Ressler: *Metall. Mater. Trans A*, 2001, **32A**, 175.
4. T. A. Palmer, J. W. Elmer and J. Wong: *Sci. Technol. Weld. Joining*, 2002, **7**, 159.
5. J. W. Elmer, T. A. Palmer, S. S. Babu, W. Zhang and T. Debroy: *J. Appl. Phys.*, 2004, **95**, 8327.
6. J. W. Elmer, T. A. Palmer, S. S. Babu, W. Zhang and T. Debroy: *Weld. J.*, 2004, **83**, 244s.
7. Z. Yang, J. W. Elmer, J. Wong and T. Debroy: *Weld. J.*, 2000, **79**, 97s.
8. W. Zhang, J. W. Elmer and T. Debroy: *Mater. Sci. Eng. A*, 2002, **333**, 320.
9. W. Zhang, J. W. Elmer and T. Debroy: *Scr. Mater.*, 2002, **46**, 753.
10. J. W. Elmer, T. A. Palmer, W. Zhang, B. Wood and T. Debroy: *Acta Mater.*, 2003, **51**, 3333.
11. A. Kumar, S. Mishra, J. W. Elmer and T. Debroy: *Metal. Mater. Trans A*, 2005, **36A**, 15.
12. W. Zhang, G. G. Roy, J. Elmer and T. Debroy: *J. Appl. Phys.*, 2003, **93**, 3022.
13. K. Mundra, T. Debroy and K. M. Kelkar: *Numer. Heat Transfer A*, 1996, **29**, 115.
14. Z. Yang, S. Sista, J. W. Elmer and T. Debroy: *Acta Mater.*, 2000, **48**, 4813.
15. S. Mishra and T. Debroy: *Acta Mater.*, 2004, **52**, 1183.
16. S. Mishra and T. Debroy: *J Phys. D: Appl. Phys.*, 2004, **37**, 2191.
17. S. Sista and T. Debroy: *Metall. Mater. Trans B*, 2001, **32B**, 1195.
18. S. Sista, Z. Yang and T. Debroy: *Metall. Mater. Trans B*, 2000, **31B**, 529.
19. H. K. D. H. Bhadeshia, L.-E. Svensson and B. Gretoft: *Acta Metall.*, 1985, **33**, 1271.
20. H. K. D. H. Bhadeshia and L. E. Svensson: in 'Mathematical modeling of weld phenomena', (ed. H. Cerjak and K. E. Easterling), 109; 1993, London, Institute of Materials.
21. Z. Yang and T. Debroy: *Sci. Technol. Weld. Joining*, 1997, **2**, 53.
22. J. W. Christian: 'The theory of transformations in metals and alloys', 1st edn; 1965, Oxford, Pergamon.
23. R. M. Miranda and M. A. Fortes: *Mater. Sci. Eng. A*, 1989, **108**, 1.
24. J. C. Ion, K. E. Easterling and M. F. Ashby: *Acta Metall.*, 1984, **32**, 1949.